Green Chemistry

PAPER

View Article Online
View Journal | View Issue

Cite this: *Green Chem.*, 2024, **26**, 2143

Mechanism study of the photothermal function of lignin: the effect of electron-withdrawing groups†

Junjie Lei,[a] Liheng Chen,[b] JinXin Lin,[b] Weifeng Liu,*[a] Qingang Xiong[c] and Xueqing Qiu*[b]

Received 26th October 2023,
Accepted 29th December 2023

DOI: 10.1039/d3gc04125e

rsc.li/greenchem

As a new type of green photothermal material, lignin exhibits an excellent photothermal effect due to its abundant aromatic rings and π–π conjugated structure. To develop value-added applications of lignin in the photothermal field, it is important to explore strategies for regulating the photothermal conversion of lignin. In this work, the photothermal effect of lignin was improved significantly through modification with an electron-withdrawing group. The introduction of acetyl resulted in the formation of an electron donor–acceptor (D–A) structure in lignin and enhanced the light absorption ability. The intermolecular interaction among lignin molecules also decreased after modification with acetyl groups, leading to enhanced non-radiative decay induced by molecular motion. Under 808 nm laser irradiation at 0.51 W cm^{-2}, the photothermal conversion efficiency of acetylated lignin (ACAL) reached as high as 73.2%, which was 37% higher than that of unmodified lignin. This study provides a new strategy to enhance the photothermal effect of lignin and deepens the understanding of the lignin photothermal mechanism.

1. Introduction

Photothermal materials represent a new class of energy-utilizing low-carbon materials. Due to their ability to absorb light and undergo photothermal conversion, photothermal materials have been used in therapy,[1] antibacterial applications,[2] catalysis,[3] and desalination.[4] Photothermal materials are divided into four categories: noble metal nanomaterials (gold nanorods and gold nanowires), transition group metal materials (MoS_2 and WS_2), carbon-based nanomaterials (carbon nanotubes and graphene oxide) and organic conjugated materials (cyanine and porphyrin).[5–7] Although photothermal materials have received extensive attention and have been the focus of research, they still exhibit some shortcomings, such as high cost, non-degradability, biological toxicity and so on. Due to the unstable structure, organic photothermal materials are susceptible to photobleaching. Besides, the synthesis of organic conjugated materials involves toxic chemical reagents. Therefore, exploring environmentally friendly, stable and efficient photothermal conversion materials is an urgent need for low-carbon sustainable development.

Biomass resources have good biocompatibility and biodegradability. The value-added utilization of biomass resources can effectively alleviate the problems of environmental pollution and resource shortage.[8] Lignin is the second largest biomass resource in the world. Technical lignin is mainly derived from the by-products of pulping and biorefining, with annual production of up to 50 million tons.[9] However, most lignin is burned or disposed and only a small portion is utilized in value-added applications.[10] Lignin is a type of amorphous aromatic natural polymer, consisting of three phenylpropane units (H, G, and S) connected by substructures (β-O-4, β-5, *etc.*), and it also contains abundant functional groups such as carboxyl, carbonyl, hydroxyl, *etc.*[11–13] Therefore, lignin exhibits excellent UV shielding,[14,15] anti-aging,[16,17] adsorption and dispersion performance.[18] As of now, lignin has been developed as an efficient water reducing agent,[19] dispersant,[20] *etc.* However, the proportion of value-added applications of lignin is still low compared to its abundant annual production. Efforts are still needed to expand the value-added application area of lignin.

Recently, researchers have found that aggregated lignin could form aromatic ring packing and π–π conjugated structures.[21] This implies that lignin could effectively absorb light and convert light energy into heat, which is helpful in developing the application of lignin in the photothermal field. For example, the photothermal function of lignin has been explored in applications such as seawater evaporation,[22] solar

[a]*State Key Laboratory of Pulp and Paper Engineering, School of Chemistry and Chemical Engineering, Guangdong Provincial Key Lab of Green Chemical Product Technology, South China University of Technology, Guangzhou 510640, China. E-mail: weifengliu@scut.edu.cn*
[b]*School of Chemical Engineering and Light Industry, Guangdong University of Technology, Guangzhou 510006, China. E-mail: qxq@gdut.edu.cn*
[c]*State Key Laboratory of Pulp and Paper Engineering, South China University of Technology, Guangzhou 510640, China*

† Electronic supplementary information (ESI) available. See DOI: https://doi.org/10.1039/d3gc04125e

power generation,[23,24] thermal management,[25] photothermal sterilization,[26] phototropic functional elastomers *etc*.[27] In recent years, few studies on the mechanism of the photothermal effect of lignin have been published. Chen *et al.* studied the photothermal effect of alkali lignin nanoparticles (L-NPs) and found that L-NPs exhibit strong absorption in the solar band and a stable photothermal conversion efficiency of 22% under a simulated solar irradiation of 100 mW cm^{-2}.[28] They also found that lignin grafted with long alkyl chains exhibited a weak photothermal effect. Chen suggested that π–π conjugation is the reason behind the photothermal conversion of lignin. Li *et al.* investigated the photothermal effect of alkaline lignin (AL), low molecular weight alkaline lignin (AOH), and enzymatic hydrolysis lignin (EL).[29] The results showed that AOH with the highest hydroxyl content exhibited the strongest photothermal efficiency of 53.7%, while EL with the lowest hydroxyl content exhibited the lowest photothermal efficiency of 27.2%. The simulation of intermolecular interactions implied that AOH had the highest binding energy while EL had the lowest, consistent with the order of the hydroxyl content. Li suggested that strong intermolecular interactions among hydroxyl groups enhanced π–π packing, leading to the strongest photothermal effect of AOH. Shao *et al.* investigated the effect of demethylation modification of lignin on its photothermal properties.[30] The modified lignin had a lower molecular weight and a higher phenolic hydroxyl content, which led to the tighter π–π packing of lignin. As a result, the modified Birch alkali lignin had a stronger light absorption capacity and a higher photothermal efficiency of 43.2%.

Tu *et al.* investigated the coordination effect on lignin photothermal conversion.[27] A significant increase in radical concentration was observed in the coordination compounds of lignin with zinc dimethacrylate (ZDMA). The lignin–ZDMA coordination compounds exhibited enhanced light absorption, decreased fluorescence emission signals and stronger photothermal conversion. Tu suggested that the coordination effect enhanced the photothermal effect of lignin by promoting radical generation. Zhao *et al.* also found that the coordination effect was beneficial for the photothermal conversion of lignin.[31] The demethylation treatment increased the phenolic hydroxyl content of lignin, which promoted the coordination of lignin with Fe^{3+}. The radical content of the coordinated lignin increased, leading to the stronger photothermal conversion of lignin. The reported literature concluded that the π–π packing of lignin was the core reason for its photothermal effect. Moreover, the enhancement of the intermolecular interaction in lignin can promote its π–π packing, which effectively strengthens its photothermal effect. In other words, these reports focused on the enhancement of the photothermal effect of lignin by promoting its molecular π–π aggregation, of which the essence was to promote the electron delocalization of the conjugated aromatic structure of lignin.

From the perspective of the molecular chemical structure, due to the conjugation effect and inductive effect, the polar functional groups of lignin, such as carboxyl and hydroxyl groups, can also change the electron cloud of the conjugated structure of lignin and thus affect the photothermal effect.[32–34] However, currently studies on the mechanism of lignin's photothermal effect have been limited to the enhancement of π–π packing, requiring further exploration of complex chemical modification and physical assembly processes for enhancing the photothermal effect. Other easier regulation strategies and a deeper mechanistic understanding of the photothermal effect of lignin are still lacking, which makes it difficult for environmentally friendly lignin to replace existing photothermal agents in various photothermal applications. Therefore, in order to explore the regulation strategies for lignin's photothermal effect as well as deepen our understanding of the mechanism, it is necessary to investigate the electronic effect of functional groups on lignin's photothermal conversion.

Photothermal conversion consists of two processes: ground-state electrons leap to a high-energy excited state through absorbing light and the excited electrons return to the ground state in non-radiative decay.[35–37] Thus, the photothermal effect can be enhanced by promoting light absorption and non-radiative decay. The light absorption ability depends on the bandgap of electron transition.[38] The main strategies to reduce the bandgap and enhance light absorption include increasing radicals,[39] constructing an extended conjugated structure[40] and introducing an electron donor–acceptor (D–A) structure.[41,43] The methods to increase radicals and construct a broad conjugated structure in lignin have been reported, while the construction of a D–A structure in lignin lacks sufficient studies. The D–A structure can reorganize original molecular orbitals and form new orbitals with a narrowed bandgap.[32,36,38] Due to the electron-donating property of methoxy and phenolic hydroxyl groups, aromatic rings of lignin should be electron-rich. Therefore, we hypothesize that grafting electron-withdrawing groups onto lignin may form a D–A structure and enhance the light absorbing properties of lignin.

Excited electrons return to the ground state through radiative decay or non-radiative decay. Photothermal conversion occurs in the latter. According to the description of the non-radiative decay mechanism, excited molecules return to the ground state through conical intersection and dissipate energy by releasing heat.[35] Strengthening π–π conjugation and molecular motion can effectively promote non-radiative decay.[36] When aggregated, the π–π packing of conjugated molecules can inhibit fluorescence radiative decay and promote non-radiative decay, known as the aggregation-caused-quenching (ACQ) effect.[43] Molecules with an extended conjugated structure, a neat planar conformation and strong intermolecular interactions can produce ordered π–π packing.[44,45] However, too tight molecular aggregation severely restricts molecular motion and is detrimental to the non-radiative decay through molecular motion.[35] Recently, researchers found that molecular motion could be strengthened by introducing a molecule rotor[46,47] and attenuating molecular aggregation.[48,49] The hydroxyl groups of lignin can form strong hydrogen bonding interactions, enhancing the π–π packing of lignin molecules.[50] However, the strong intermolecular interaction restricts the

molecular motion of lignin. Therefore, weakening intermolecular interactions and strengthening molecular motion by substituting the hydroxyl groups of lignin may improve non-radiative decay and promote the photothermal conversion of lignin.

We hypothesized that the photothermal effect of lignin could be regulated by modifying lignin with an electron-withdrawing group, where the group plays two roles: on the one hand, the D–A structure formed by electron-donating aromatic rings and the electron-withdrawing group would enhance the light absorbing properties of lignin; on the other hand, the substitution of hydroxyl groups by electron-withdrawing groups would decrease intermolecular interactions within lignin and enhance its nonradiative relaxation through molecular motion. In this work, we prepared three modified alkali lignins, including acetylated lignin (ACAL), ethylated lignin (EAL) and dodecylated lignin (DAL). The electronic effects of functional groups and the change of intermolecular interaction on the photothermal effect of lignin were studied. The mechanism by which electron-withdrawing groups enhance the photothermal conversion of lignin was revealed. This study demonstrated that in addition to π–π conjugation, the functional groups and the intermolecular interaction were also important factors affecting the photothermal conversion of lignin, which provided new strategies for regulating the photothermal effect of lignin.

2. Experiment section

2.1 Materials

Alkali lignin (AL) was provided by Shanghai Changfa New Materials Co., Ltd (China). Acetyl chloride was purchased from Shanghai Aladdin Biochemical Technology Co., Ltd (China). Acetic acid, bromoethane and 1-bromododecane were purchased from Shanghai Energy Chemical Co., Ltd (China). Potassium iodide (KI) was purchased from Shanghai AI LAN Chemical Technology Co., Ltd (China). Sodium hydroxide (NaOH) was purchased from Tianjin Fuchen Chemical Reagent Co., Ltd (China). Sulfuric acid was purchased from Guangzhou Chemical Reagent Factory (China). All of the chemical reagents except for lignin were of AR grade.

2.2 Preparation of ACAL, EAL and DAL

2.2.1. Acetylated lignin (ACAL). Alkali lignin (10.0 g) was added into a three-necked flask. Acetyl chloride (40 mL) and acetic acid (160 mL) were mixed in a 1 : 4 ratio by volume and added into the flask. The reaction was carried out at 40 °C for 2 h. After reaction completion, the residual solvent was removed using a rotary evaporator. Then, the resulting product was mixed with deionized water and purified by centrifugation. Finally, the precipitated solid product was collected and dried under vacuum at 55 °C for 24 h.

2.2.2. Ethylated lignin (EAL). Alkali lignin (12.0 g) was added into a three-necked flask. 4% NaOH solution (130 mL) and ethanol (85 mL) were mixed and added into the flask. Then, bromoethane (4.5 mL) and KI (0.10 g) were added into the flask. The reaction was carried out at room temperature for 24 h. After reaction completion, the residual bromoethane was extracted with petroleum ether. Then, the product was precipitated using 20% sulfuric acid and washed with deionized water. Finally, the solid product was dried under vacuum at 55 °C for 24 h.

2.2.3. Dodecylated lignin (DAL). Alkali lignin (12.0 g) and 4% NaOH solution (200 mL) were mixed and added into a flask. Then, 1-bromododecane (15.0 g) and KI (0.10 g) were added into the flask. The reaction was carried out at 85 °C for 5 h. After reaction completion, the residual bromododecane was extracted with petroleum ether. Then, the product was precipitated using 20% sulfuric acid and washed with deionized water. Finally, the solid product was dried under vacuum at 55 °C for 24 h.

2.3 Characterization

Fourier transform infrared (FT-IR) spectra of all lignin samples were recorded using Nicolet IS50 – Nicolet Continuum (Nicolet, America). Lignin powder was mixed with KBr for tablet pressing and tested in the transmission mode. The scanning wave number ranged from 4000 to 400 cm^{-1} with 16 scans.

^{1}H NMR spectra were recorded using AVANCE NEO 500 MHz (Bruker, Germany). The scanning frequency was 500 MHz. Lignin powder (30 mg) was dissolved in DMSO-d_6 (0.6 mL) and tested.

Quantitative ^{31}P NMR spectra and two-dimensional heteronuclear single quantum coherence (2D-HSQC) NMR spectra were recorded using AVANCE III HD 600 (Bruker, Germany). Lignin powder (30 mg) was dissolved in DMSO-d_6 (0.6 mL) for 2D-HSQC NMR spectral analysis. The preparation of the sample for ^{31}P NMR is as follows: the solvent was prepared with anhydrous deuterated pyridine and anhydrous deuterated chloroform in a volume ratio of 1.6/1. Lignin (30 mg) was dissolved in the solvent (0.5 mL). The internal standard solution was prepared using *N*-hydroxy-5-norbornene-2,3-dicarboxylic imide (0.018 g) as the internal standard, chromium(III) acetylacetonate (0.005 g) as the relaxation agent and the solvent (1 mL). Then, 0.10 mL of this internal standard solution was added to the abovementioned solution. The homogeneous mixture was transferred to a nuclear magnetic tube and the phosphating reagent 2-chloro-4,4,5,5-tetramethyl-1,3,2-dioxaphospholane (0.15 mL) was added to obtain the test sample. The formula for calculating the hydroxyl content of lignin is as follows:

$$c_{OH}(\text{mmol g}^{-1}) = \frac{m_1}{179.17} \times 0.99 \times 1000 \times \frac{m_{IS}}{m_1 + m_2 + m_3} \times \frac{A_{OH}}{A_{IS} \times m_L}$$

where c_{OH} (mmol g^{-1}) is the content of lignin hydroxyl groups, m_1 (g) is the mass of the internal standard, m_2 is the mass of the relaxation agent, m_3 is the mass of the as prepared internal standard solution, m_{IS} is the mass of the internal standard solution added into the test sample, m_L is the mass of lignin, A_{OH} is the peak area of the hydroxyl group, A_{IS} is the peak area of the internal standard.

Ultraviolet–visible–near-infrared (UV-vis-NIR) absorption spectra were recorded using UV-2600i (Shimadzu, Japan). The test mode was attenuated total reflection (ATR). The scanning range was from 200 to 1200 nm.

Fluorescence and phosphorescence spectra were recorded using F-7000 (Hitachi, Japan). The excitation wavelength was 808 nm and the collection wavelength was from 828 to 900 nm.

Scanning electron microscopy (SEM) of lignin-coated SiO_2 particles was conducted using SU-8200 (Hitachi, Japan). One drop of lignin solution was dropped onto a silicon wafer and dried at room temperature for testing.

Differential scanning calorimetry (DSC) was conducted using a Netzsch 214 instrument (Netzsch, Germany) with nitrogen as the atmospheric gas. The test parameters for lignin's specific heat capacity were as follows: the temperature range was from 20 to 250 °C, and the heating rate was 10 °C min^{-1}. The test parameters for the glass transition of lignin were as follows: the temperature range was from −60 to 200 °C, and the temperature increase rate was 10 °C min^{-1}.

Atomic force microscopy (AFM) force spectroscopy was conducted using XE-100 (Park Systems, Korea). The AFM probe and the substrate were modified using the same lignin sample. In detail, SiO_2 particles were immersed in Piranha solution (98% sulfuric acid and 30% H_2O_2 solution in a 7 : 3 ratio by volume) to generate more negative charges. Then, SiO_2 particles were immersed in PDAC solution (20 g L^{-1}), followed by immersion in a lignin alkali solution (2 g L^{-1}). The lignin-coated AFM probe was obtained by attaching lignin-coated SiO_2 particles to a tipless AFM cantilever. The lignin-coated substrate was modified using a similar method except that lignin was attached to the surface by spin coating. Force spectroscopy measurements were performed in a 3.0 × 3.0 cm^2 glass dish filled with deionized water at room temperature. The test parameters used during all force spectroscopy measurements were as follows: the limited force was 10.0 nN, the set point was 3.0 nN, and the limited force distance was 2.0 μm. Every force spectroscopy measurement was carried out 200 times at different locations on the substrate.

2.4 Measurement of photothermal conversion of modified lignin

2.4.1 Continuous irradiation with an 808 nm laser at different power densities. The lignin powder was pressed into discs. The samples were continuously irradiated with an 808 nm laser (Lasever, China) at 0.14, 0.33, 0.51, 0.81, and 1.00 W cm^{-2} for 4 min. Before irradiating at the next power density, the laser was switched off for 3 min. The maximum temperature changes on the surface of lignin were recorded using an infrared camera (FLIR, America). The distance between the sample and the laser was fixed at 10 cm. The distance between the sample and the infrared camera was fixed at 20 cm. The power density was obtained by dividing the power by the irradiated area. The power was measured using an optical power meter (PerfectLight, China). The irradiated area was a circular spot with a diameter of 6 mm. Photothermal heating curves were obtained for irradiation at consecutively different light power densities.

2.4.2 Cyclic on/off irradiation with an 808 nm laser at a constant light power. The sample was irradiated with an 808 nm laser at 0.81 W cm^{-2} for three consecutive on/off irradiation cycles. During each cycle, the laser was switched on for 4 min and switched off for 3 min. The maximum temperature changes on the surface of lignin were recorded using an infrared camera. Photothermal heating curves were obtained for cyclic irradiation at a constant laser power density.

2.5 Simulation methods

Molecular simulation for lignin clusters (containing two monomers) was carried out using the molecular dynamics (MD) module of the extended tight binding (xTB) program to generate thousands of configurations. All generated structures were pre-optimized at the GFN0-xTB level and re-optimized at the GFN2-xTB level to collect the configurations with an energy difference of less than 5 kcal mol^{-1} from the least energetic structure using the Molclus software. The collected configurations were then optimized and the frequencies were calculated at the B3LYP-D3(BJ)/6-31G* level to obtain the configurations with the lowest energy using the Gaussian 16 software. The interaction energy between the monomers was calculated at the RI-PWPB95-D3(BJ)/def2-QZVPP level using the ORCA 4.2 software. Non-covalent interactions (NCIs) were analyzed using the independent gradient model based on the Hirshfeld partition (IGMH) method *via* the Multiwfn 3.8 (dev) program. The orbital structures and NCIs of the monomers were visualized using the VMD 1.9.3 package.

3. Results and discussion

3.1 Synthesis and characterization of modified lignin

As shown in Fig. 1, the electron-withdrawing acetyl group and the electron-donating ethyl and dodecyl groups were introduced through substituting the phenolic hydroxyl and alcoholic hydroxyl groups in lignin, which were named ACAL, EAL and DAL, respectively. To confirm the structure of the modified lignin, FTIR analysis of pristine lignin (AL) and modified

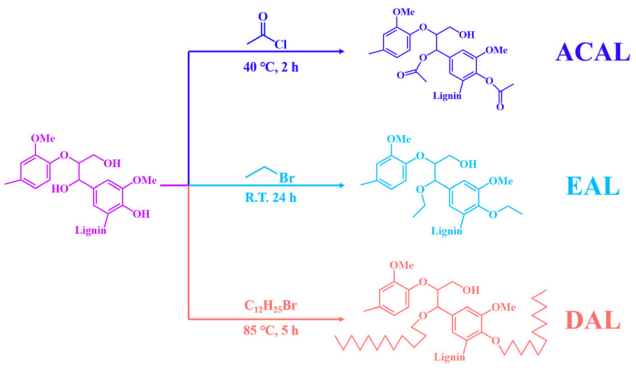

Fig. 1 Illustration of lignin modification.

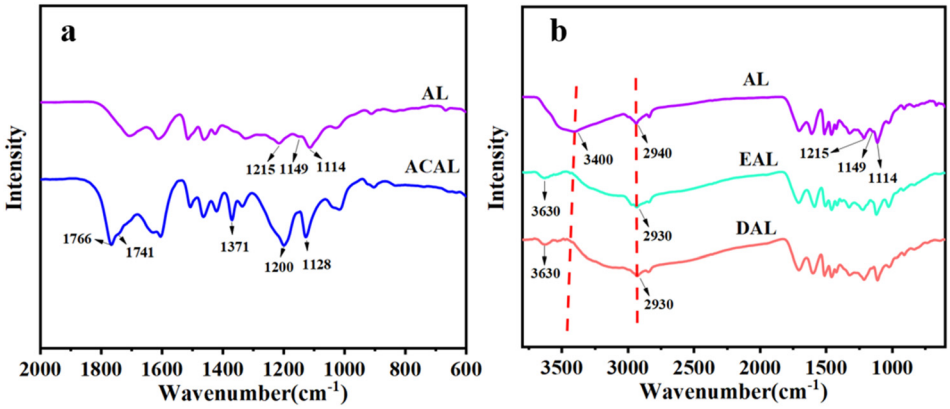

Fig. 2 (a) FTIR spectra of AL and ACAL. (b) FTIR spectra of AL, EAL and DAL.

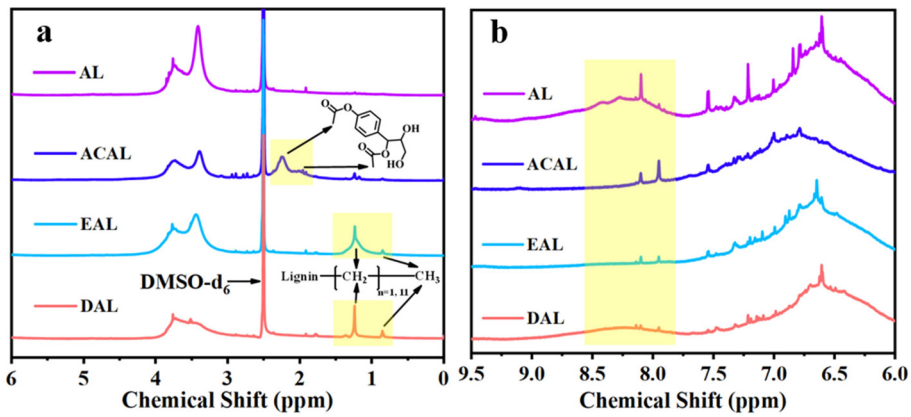

Fig. 3 (a) ^{1}H NMR spectra of lignin ranging from 0 to 6.0 ppm. (b) ^{1}H NMR spectra of lignin ranging from 6.0 to 9.5 ppm.

lignin was carried out. As shown in Fig. 2a, the absorption peaks at 1766 and 1741 cm^{-1} in ACAL corresponded to the side-chain carboxylate and aromatic carboxylate, respectively.[51,52] The peak at 1371 cm^{-1} in ACAL was attributed to acetyl. The absorption peaks of AL at 1215, 1149 and 1114 cm^{-1} corresponded to phenolic hydroxyl groups, and tertiary and secondary alcoholic hydroxyl groups, respectively. In the spectrum of ACAL, these three peaks were weakened. Moreover, strong peaks appeared at 1200 and 1128 cm^{-1} in ACAL, attributed to the enhanced stretching vibration of the ester C–O bond. As shown in Fig. 2b, the absorption peaks attributed to the hydroxyl stretching vibration at 3400 cm^{-1} were significantly weakened in EAL and DAL and shifted to a higher wavenumber, indicating the reduced hydroxyl groups and hydrogen bonds in EAL and DAL.[53,54] Both EAL and DAL had a significantly enhanced peak at 2930 cm^{-1}, attributed to the methyl and methylene groups. The absorption peaks of phenolic and alcoholic hydroxyl groups at 1200–1100 cm^{-1} in EAL and DAL significantly weakened. The FTIR analysis verified the successful modification of lignin.

The chemical structure of the modified lignin was further verified by ^{1}H NMR. As shown in Fig. 3a, ACAL had strong peaks at 2.24 and 1.96 ppm, corresponding to the acetyl proton signals at the reaction sites of phenolic hydroxyl and alcoholic hydroxyl groups, respectively.[52] The peaks at 1.22 and 0.84 ppm in EAL and DAL corresponded to the proton signals of methylene and methyl groups, respectively.[54] Fig. 3b showed a broad peak at 8.0–9.0 ppm in AL, attributed to the phenolic hydroxyl group.[52] In the ^{1}H NMR spectra of ACAL, EAL and DAL, this peak was significantly weakened, indicating that the content of phenolic hydroxyl groups was reduced after the modification reaction. To quantitatively analyze the changes in the hydroxyl group content, ^{31}P NMR spectra were characterized and the result is presented in Table 1. The alcoholic and phenolic hydroxyl group content of all modified lignins decreased. These results demonstrate that acetyl, ethyl and dodecyl groups were successfully substituted with the alcoholic and phenolic hydroxyl groups of lignin.

Table 1 Hydroxyl group content of lignins

	AL	ACAL	EAL	DAL
Alcoholic OH (mmol g^{-1})	0.39	0.03	0.30	0.15
Phenolic OH (mmol g^{-1})	1.69	0.03	0.68	1.55

The detailed molecular structure of lignin was further characterized by 2D-HSQC NMR analysis. Fig. 4a and c show that the substructures of AL consisted of β-O-4, β-5 and β–β, resolved by the Cα–Hα correlation signals at δC/δH 72.5/4.86, 87.5/5.41, and 85.5/4.64, respectively.[28] The distribution of the basic unit composition of lignin was obtained

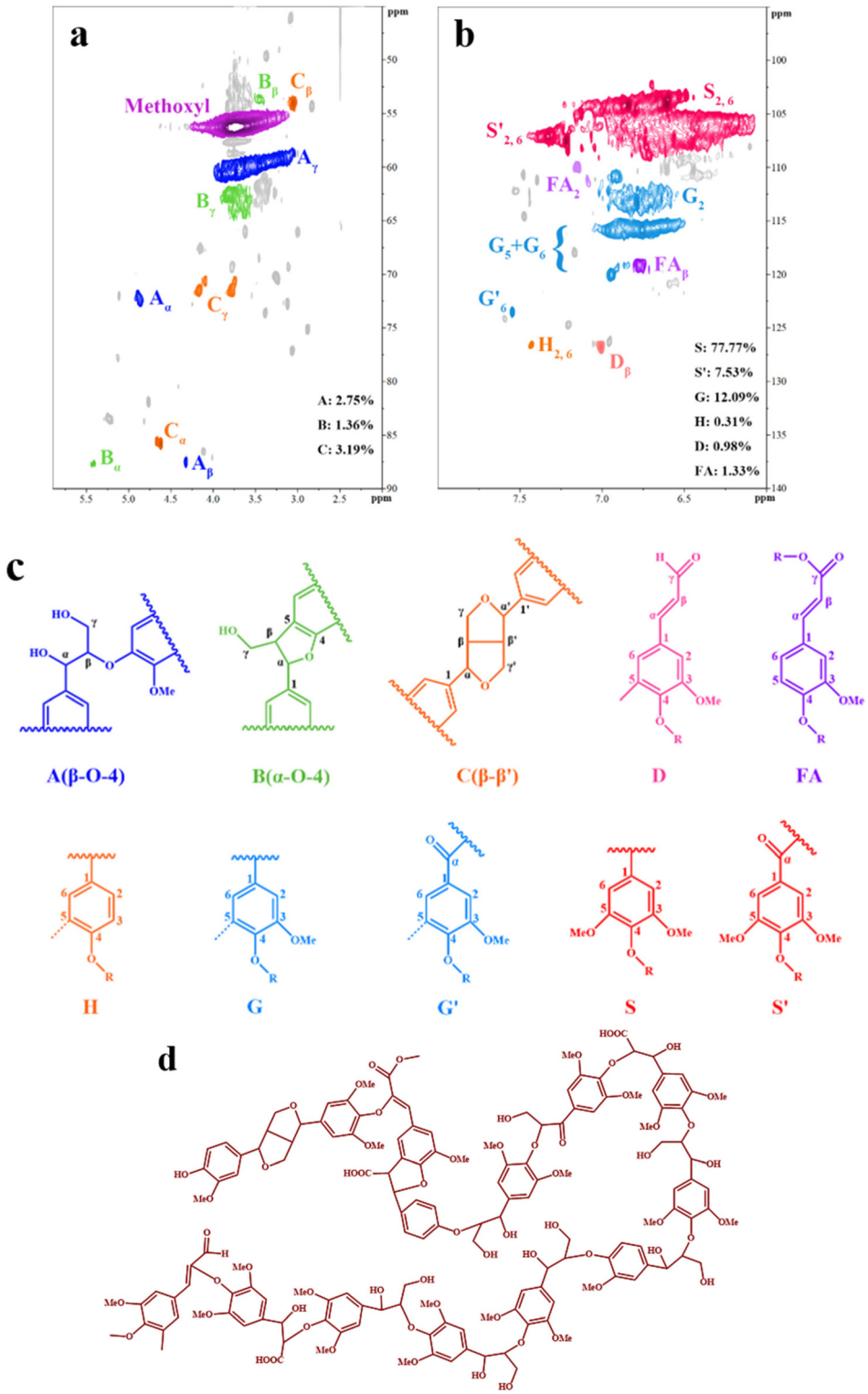

Fig. 4 (a) 2D-HSQC NMR spectra of the substructures of AL. (b) 2D-HSQC NMR spectra of the basic units of AL. (c) Substructures and basic units present in AL: A: β-O-4; B: β-5; C: β–β′; D: cinnamyl aldehyde end-groups; FA: ferulate; H: *p*-hydroxyphenyl; G: guaiacyl units; G′: oxidized guaiacyl unit bearing a carbonyl group at Cα; S: syringyl unit; S′: oxidized syringyl unit bearing a carbonyl group at Cα. (d) The molecular structure fragment model of AL.

by integrating the signals of different structural units, as shown in Fig. 4b and c.[55–57] The basic units of AL were mainly composed of a syringyl unit (S and S′ about 85%). Based on the analysis of 2D-HSQC NMR spectra, a molecular structure fragment model was constructed for AL, as shown in Fig. 4d. In the subsequent molecular simulation, we will extract fragments from the molecular structure as model objects.

3.2 Photothermal effect of modified lignin

An 808 nm near-infrared laser was used to induce the photothermal conversion of lignin. The lignin sample was continuously irradiated with the laser at a power density ranging from 0.14 W cm^{-2} to 1.00 W cm^{-2} and the maximum temperature of the sample surface was recorded using an infrared camera. As shown in Fig. 5a, ACAL had the highest surface maximum

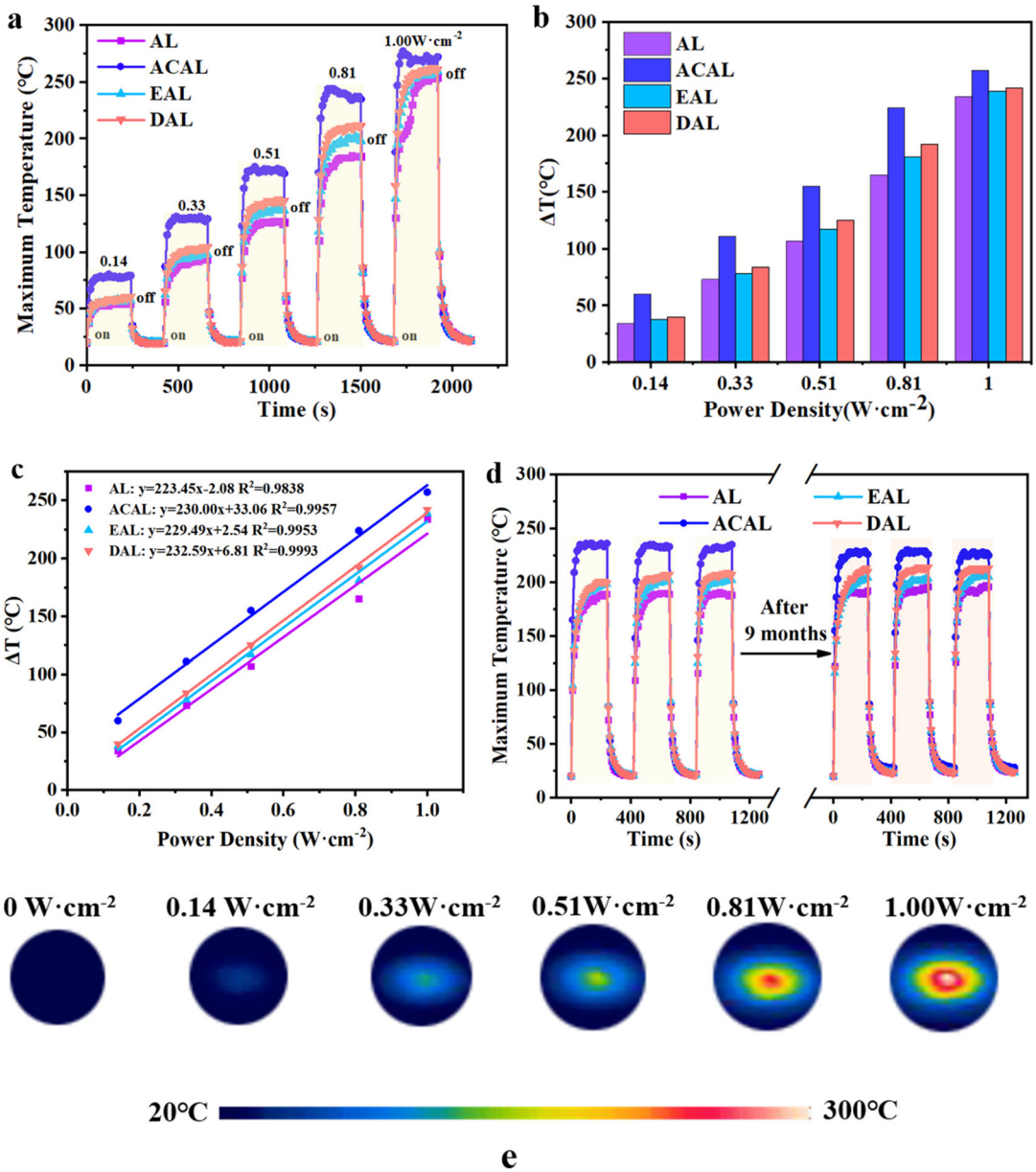

Fig. 5 (a) Surface temperature change of lignin through alternative switch-on and -off 808 nm laser irradiation at different power densities (W cm^{-2}). (b) The maximum temperature increment, ΔT, of lignin under 808 nm laser irradiation at different power densities (W cm^{-2}). (c) The maximum temperature increment, ΔT, of lignin *versus* the light power density (808 nm). (d) The photothermal stability measurement of lignin through alternative heating and cooling (3 cycles) by switching-on and -off 808 nm laser radiation at 0.81 W cm^{-2}; the durability of the modified lignin in the enhancement of photothermal effect was verified by photothermal measurements after 9 months. (e) Infrared thermal imaging images of ACAL under 808 nm laser irradiation at different light power densities: 0 W cm^{-2}, 0.14 W cm^{-2}, 0.33 W cm^{-2}, 0.51 W cm^{-2}, 0.81 W cm^{-2}, and 1.00 W cm^{-2}.

temperature, indicating the strongest photothermal effect among the studied lignins. The surface maximum temperature of EAL was slightly higher than that of AL. Interestingly, compared with that of AL, the surface maximum temperature of DAL modified with long-chain dodecyl groups also increased significantly. This result was contrary to the previous report,[28] and this phenomenon will be discussed in the following section. Fig. 5b shows that the temperature increment, ΔT, of ACAL was significantly higher than that of AL. Under the laser irradiation at 0.81 W cm^{-2}, the temperature increment, ΔT, of ACAL reached 224 °C, while it was only 165 °C for AL. A good linear relationship between the temperature increment and the light power density was observed, as shown in Fig. 5c, indicating that the temperature increment, ΔT, could be accurately controlled by modulating the light power density. The lignin sample was repeatedly irradiated with the laser at 0.81 W cm^{-2} to test the photothermal stability. Fig. 5d shows that the temperature increment of all lignins did not change significantly, and all lignins maintained an excellent photothermal temperature increment even after 9 months, demonstrating the excellent stability and durability of photothermal heating. The photothermal conversion efficiency of AL, ACAL, EAL and DAL was calculated under the laser irradiation at 0.51 W cm^{-2}. The specific heat capacity C_p and cooling time τ_s used to calculate the photothermal conversion efficiency are shown in Fig. S1 and Table S1.† The photothermal conversion efficiencies of AL, EAL, DAL and ACAL were 53.6%, 54.5%, 56.3% and 73.2%, respectively (Table S1†). Compared to that of AL, the photothermal efficiency of ACAL was improved by 37%. These results demonstrate that the electron-withdrawing acetyl group could significantly enhance the photothermal effect of lignin, in comparison with the electron-donating ethyl and dodecyl groups. In particular, the photothermal conversion efficiency of 73.2% for ACAL exceeded those of most of the organic photothermal materials (Table S2†).

3.3 Long-wavelength absorption of modified lignin

To reveal the mechanism of photothermal enhancement in modified lignin, the effect of functional groups on the light absorption ability of lignin was analyzed, as shown in Fig. 6. Compared to AL, the color of modified lignins deepened (Fig. 6a), implying stronger light absorption. The UV-vis-NIR absorption spectra shown in Fig. 6b indicate that the light absorption ability of ACAL and DAL significantly improved in the visible and near-infrared bands. At 808 nm, the absorption of ACAL and DAL was twice as high as that of AL, while EAL had a slightly higher absorption than AL. The light absorption difference of ACAL and EAL indicated that the electron-withdrawing acetyl group was more effective in narrowing the electron transition bandgap and enhancing the light absorption than the electron-donating ethyl group. According to our hypothesis, the introduction of acetyl might result in the formation of a D–A structure. According to previous reports, side groups with large steric hindrance inhibit the π–π packing of lignin and weaken the photothermal effect.[28] However, in this work, DAL modified with long-chain dodecyl groups showed a contrasting phenomenon, that is, the enhanced light absorption and photothermal effect. As both ethyl and dodecyl groups are electron-donating groups, the striking light absorption difference between EAL and DAL indicated that the electron-donating effect was not the key factor for the enhanced light absorption of DAL. We suggested that the enhancement of the light absorption and photothermal effect in DAL might be due to the molecular aggregation. After modification, DAL aggregated during acid precipitation. The strong hydrophobic dodecyl group enhanced the intermolecular interaction and resulted in a closer π–π packing of DAL, which strengthened the light absorption and photothermal conversion of DAL.[53,54] We will verify this hypothesis in the subsequent section. The difference of light absorption indicated that the electron-withdrawing effect could effectively improve the light absorption ability of lignin.

The effect of functional groups on the absorption bandgap of lignin was studied through calculating the molecular orbital energy level and electron cloud distribution. As shown in Table 2, the energy levels of the lowest unoccupied molecular orbital (LUMO), the highest occupied molecular orbital (HOMO) and the bandgap of AL were −0.16 eV, −5.74 eV and 5.58 eV, respectively. The energy levels of LUMO, HOMO and the band gap of ACAL were −0.60 eV, −5.94 eV and 5.34 eV, which decreased by 0.44 eV, 0.20 eV and 0.24 eV, respectively, compared to those of AL. The decrease in the LUMO–HOMO gap energy of ACAL indicated the formation of a D–A structure. The grafting of the electron-withdrawing acetyl group onto lignin resulted in the formation of the D–A structure, as the molecular orbitals of the aromatic ring (donor) and the acetyl group (acceptor) could recombine and form new molecular orbitals with a narrower bandgap.[32] The decrease of LUMO energy was larger than that of HOMO energy, resulting in the narrowed bandgap of ACAL. In addition, the electron cloud distribution image of ACAL shown in Table 2 exhibits a typical charge transfer characteristic of a D–A structure: the electron cloud of the HOMO was concentrated in the electron-donating aromatic ring, and the electron cloud of the LUMO was concentrated in the electron-accepting acetyl group.[41,42] The change in the energy level of molecular orbitals and the electron cloud transfer verified that ACAL narrowed the bandgap

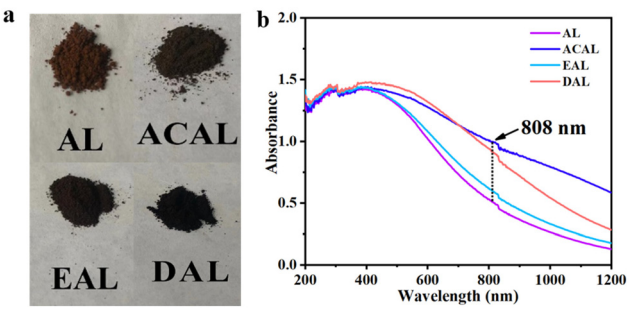

Fig. 6 (a) Sample photos of lignin, (b) UV-vis-NIR spectra of lignin samples ranging from 200 to 1200 nm.

Table 2 Calculated energy and molecular orbits of lignins

	AL	ACAL	EAL	DAL
Molecular structure	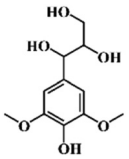	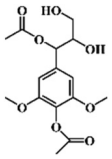	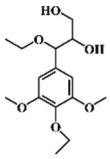	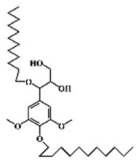
LUMO	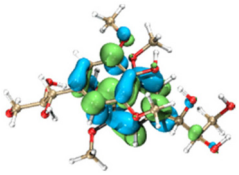	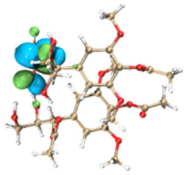	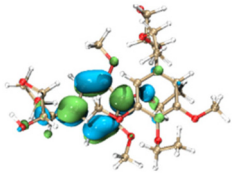	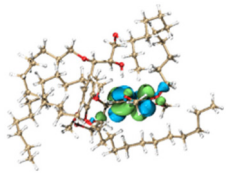
HOMO	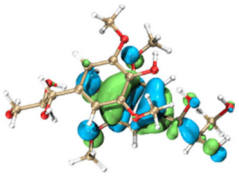	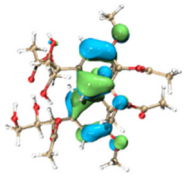	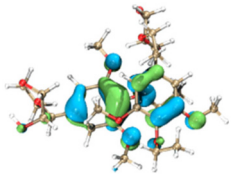	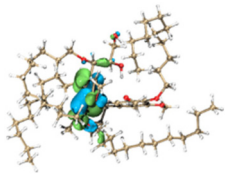
Bandgap	5.58 eV	5.34 eV	5.53 eV	5.60 eV

and enhanced the light absorption through forming the D–A structure. The energy levels of the LUMO, HOMO and bandgap of EAL were −0.02 eV, −5.55 eV and 5.53 eV, respectively. Compared to those of AL, both LUMO and HOMO of EAL increased. This indicated that the molecular orbitals of EAL also recombined. However, weak electron-donating ethyl groups failed to form a D–A structure and transfer electron cloud. As a result, the bandgap of EAL was slightly narrowed. The bandgap of DAL was 5.60 eV, similar to that of AL. Like ethyl, the weak electron-donating effect of dodecyl also failed to narrow the bandgap of DAL. This indirectly indicated that the light absorption enhancement in DAL was not attributed to the electron effect, but might be due to the aggregation enhancement of π–π packing. The calculation of the molecular orbital energy level verified that the electron-withdrawing effect could narrow the bandgap and enhance the light absorption of lignin through forming a D–A structure.

3.4 Non-radiative decay of modified lignin

Because of the competitive relationship between radiative decay and non-radiative decay, the fluorescence and phosphorescence emission can indirectly reflect the non-radiative decay of lignin. The fluorescence and phosphorescence emission spectra of modified lignin excited by an 808 nm laser were recorded. As shown in Fig. 7a, the fluorescence emission signals of ACAL, EAL and DAL obviously decreased compared to those of AL. In Fig. 7b, no significant phosphorescence signals were detected for all lignins. The emission spectra indicate that the radiation decay of modified lignin was weakened and the non-radiation decay enhanced accordingly.[35] This was consistent with the change in photothermal heating. The hydroxyl groups of pristine lignin formed strong intermolecular interactions; thus, the π–π aggregation of lignin was strengthened and inhibited radiation decay through the ACQ effect.[29] However, the close aggregation of lignin severely restricted the molecular motion and inhibited non-radiative decay through molecular motion. The modification of lignin consumed the hydroxyl groups, which could attenuate lignin aggregation and enhance the molecular motion. Therefore, the radiative decay of the ACAL and EAL modified with short-chain groups was weakened, and their photothermal non-radiative decay was enhanced. Although the reaction site of DAL was the hydroxyl group, resulting in reduced hydrogen bonds, we speculated that the diminished radiative decay of DAL was due to the hydrophobic aggregation of dodecyl, leading to enhanced intermolecular interaction and π–π packing. Next, to verify the hypothesized mechanism of the non-radiative decay enhancement in modified lignin, we characterized the molecular motility and intermolecular interaction in lignin.

In order to observe the molecular motility of lignin, the glass transition temperature, T_g, of lignin was characterized. The glass transition indicates that the frozen polymer chains can undergo molecular chain torsion or other molecular motions when gradually heated to the T_g. The T_g is generally associated with the rigidity of polymer chains and intermolecular interactions. Polymer materials with rigid chain segments and stronger intermolecular interactions usually have a higher T_g. Fig. 7c shows that the T_g of AL was 177.1 °C, while the T_g of ACAL and EAL decreased to 170.8 °C and 167.0 °C, respectively. The T_g of DAL increased significantly, reaching 212.2 °C. The above results reflected the weakened intermolecular interaction in ACAL and EAL and the enhanced intermolecular interaction in DAL, compared to that of AL. The strong hydrogen bonds of pristine lignin promoted aggregation and restricted molecular motion. After modification, the hydroxyl groups in modified lignin decreased, and the

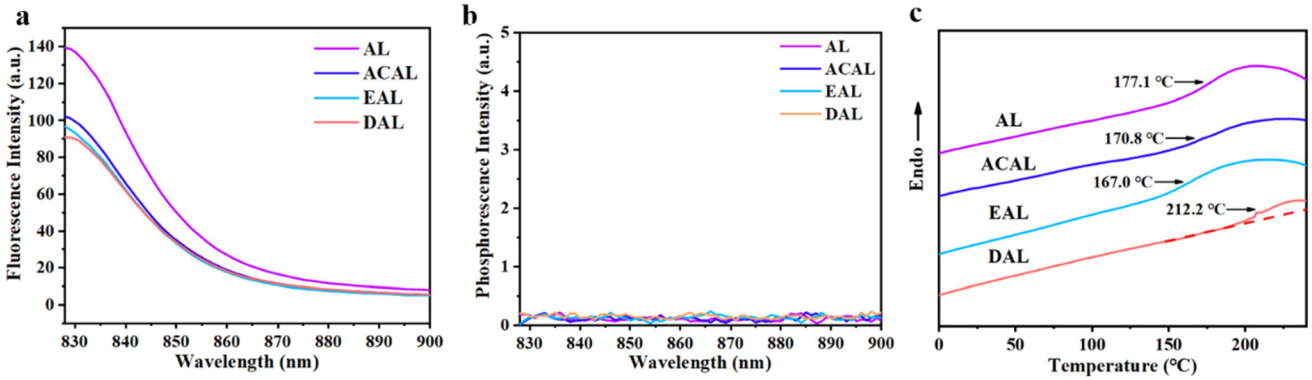

Fig. 7 (a) Fluorescence emission spectra of lignin excited by 808 nm NIR, (b) phosphorescence emission spectra of lignin excited by 808 nm NIR, and (c) DSC curve of lignin.

molecular mobility enhanced. As a result, the molecular motion of ACAL and EAL was strengthened, leading to the enhanced non-radiative decay. The hydroxyl groups in DAL also decreased; however, the increase of T_g indicated that the total intermolecular interaction in DAL significantly enhanced. This might be attributed to the fact that the strong hydrophobicity of dodecyl outweighed the effect of hydrogen bond reduction, resulting in an enhanced total intermolecular interaction in DAL. The enhancement of intermolecular interaction could strengthen the π–π packing of DAL, which promoted light absorption but inhibited non-radiative decay through molecular motion. Thus, the photothermal effect of DAL was stronger than that of AL but weaker than that of ACAL.

To quantify the change in intermolecular interaction, atomic force microscopy (AFM) was used to characterize the adhesion force of lignin molecules. As shown in Fig. 8a, the silicon probe and the quartz substrate were modified with the same lignin sample. The change of adhesion force between the probe and the substrate was recorded as the probe was moved away from the substrate. Fig. S2† shows sufficient lignin adhesion on the probe surface for testing. Fig. 8b and c show that the average adhesion force among AL molecules was −92.10 μN m^{-1}. The average adhesion force among ACAL molecules and EAL molecules decreased to −46.80 μN m^{-1} and −11.03 μN m^{-1}, respectively. The average adhesion force among DAL molecules increased to −213.52 μN m^{-1}, which was 2.3 times higher than that of AL molecules. The adhesion force is the overall manifestation of intermolecular interactions among lignin molecules, including hydrogen bonding, hydrophobic interaction, electrostatic interaction and van der Waals interaction. The hydroxyl content of ACAL and EAL decreased significantly, resulting in weakened hydrogen bonds. As a result, the intermolecular interaction between ACAL and EAL decreased. Although the hydrogen bonds of DAL decreased, the strong hydrophobic interaction of dodecyl significantly increased the total intermolecular interaction in DAL. This result verified the above hypothesis that the strong hydrophobic interaction in dodecyl strengthened the aggregation of DAL during the post-treatment process, resulting in a closer π–π packing.

The intermolecular interaction in lignin was also calculated by the foregoing MD simulations, using the molecular fragments as models. As shown in Table 3, the intermolecular interaction energy of AL models was −20.76 kcal mol^{-1}. The negative intermolecular interaction energy indicated that AL models tended to aggregate, and the larger absolute value implied the stronger aggregation of lignin models. Due to the reduction of hydroxyl groups, the intermolecular interaction energy of ACAL models increased to −18.08 kcal mol^{-1}, improved by 2.68 kcal mol^{-1} compared to that of AL. Due to the strong hydrophobic interaction of dodecyl, the intermolecular interaction energy of DAL models decreased to −37.54 kcal mol^{-1}, in which their interaction was about 1.8 times higher than that of AL. From the NCI iso-surface of DAL, the abundant interaction of dodecyl molecular chains was also observed, represented by a green contour plane between molecular chains. The intermolecular interaction energy (−21.19 kcal mol^{-1}) of EAL models was slightly lower than that of AL (−20.76 kcal mol^{-1}). On the whole, the order of calculated intermolecular interaction in lignin was consistent with the results obtained from DSC and AFM. These results demonstrated that the intermolecular interaction in ACAL and EAL was weakened by substituting hydroxyl groups. It was also verified that strong hydrophobic dodecyl groups enhanced the intermolecular interaction in DAL, leading to a closer π–π packing.

3.5 Mechanism of the enhanced photothermal effect of modified lignin

Based on the above results, we proposed the mechanism by which the electron-withdrawing groups enhance the photothermal effect of lignin, as shown in Fig. 9. By introducing the electron-withdrawing group acetyl, the D–A structure was successfully constructed in lignin molecules. This resulted in the narrowed bandgap and enhanced the light absorption capacity of ACAL. After modification, the hydroxyl content of ACAL

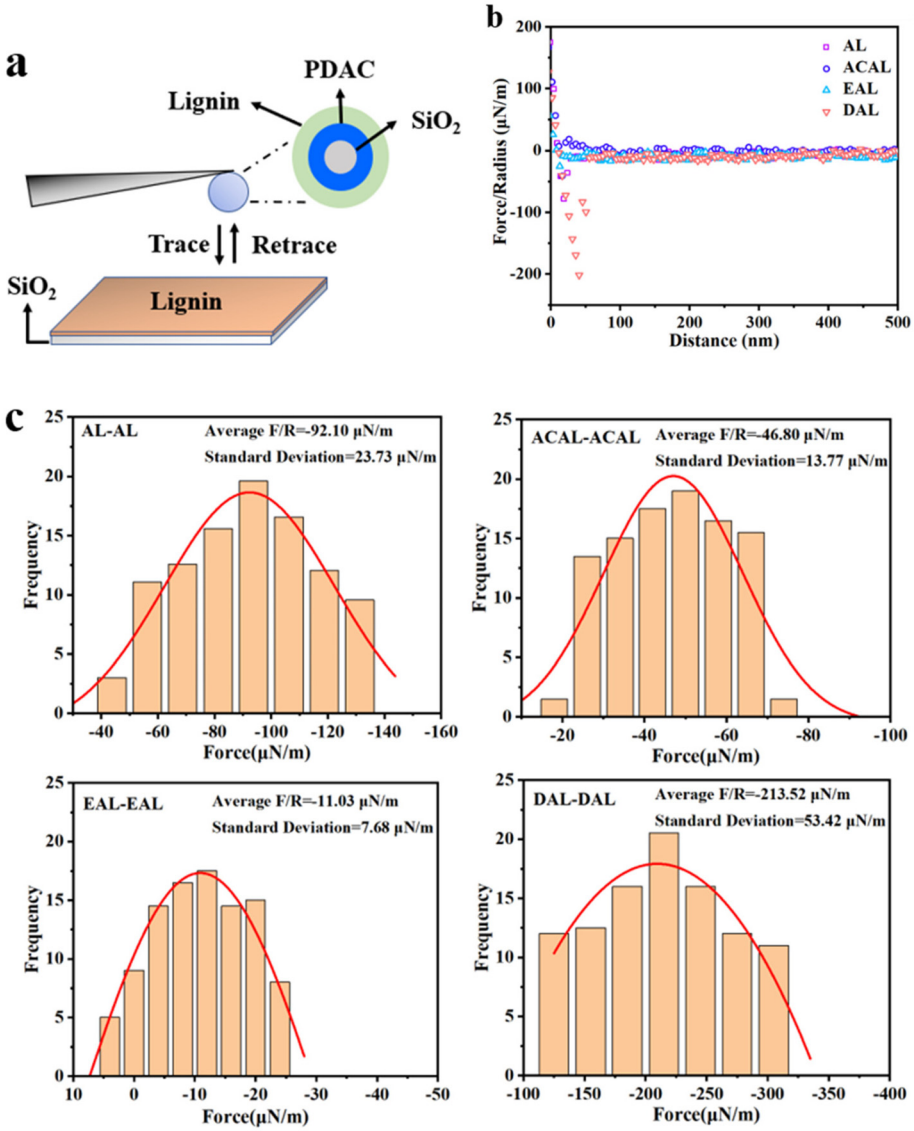

Fig. 8 (a) Schematic diagram of the spherical probe coated with lignin for AFM force measurements in water. (b) Typical AFM force–distance retraction curves of lignin. Adhesion forces can be obtained from the retraction curve. Positive and negative values represent repulsive and attractive forces, respectively. (c) Schematic diagram of the histogram of AFM-measured adhesion forces of lignin.

decreased, leading to the reduction of hydrogen bonds. Thus, the intermolecular interaction of ACAL was weakened and the molecular motion was enhanced. The enhanced molecular motion promoted the non-radiative decay of ACAL, ultimately facilitating the photothermal conversion. Due to the enhancement of both light absorption and non-radiative decay, ACAL exhibited the strongest photothermal effect. The strong hydrophobic dodecyl group significantly improved the intermolecular interaction in DAL and promoted π–π aggregation. Thus, the light absorption of DAL was enhanced. Meanwhile, the molecular motion of DAL was severely limited, inhibiting the non-radiative decay through molecular motion. Therefore, the photothermal efficiency of DAL was higher than that of AL but lower than that of ACAL. Due to the weak electron-donating effect of ethyl, EAL could not promote light absorption through forming a D–A structure. But the substitution of hydroxyl by ethyl weakened the intermolecular interaction in EAL and promoted non-radiative decay through molecular motion. As a result, the photothermal effect of EAL is slightly stronger than that of AL. In short, the enhancement of both light absorption and molecular motion is beneficial for the photothermal effect of lignin.

In the reported literature, the photothermal effect of lignin was enhanced by strengthening the π–π packing *via* chemical modification and physical assembly processes. However, the former required high energy-consumption reaction conditions (high temperature and long reaction time), *e.g.* 150 °C and 12 h, and used environmentally unfriendly organic solvents, *e.g.*, *N*,*N*-dimethylformamide used in demethylation modification.[30] The latter required precise control of the assembly

Table 3 Calculated interaction energy of lignins

	AL	ACAL	EAL	DAL
Molecular structure	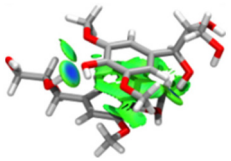	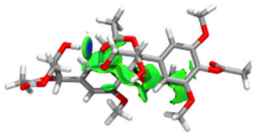	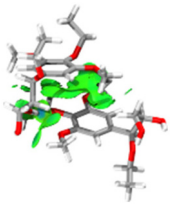	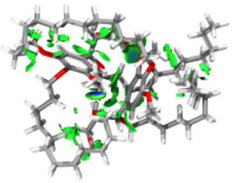
Boltzmann distribution	50%	99%	100%	84%
Interaction distribution	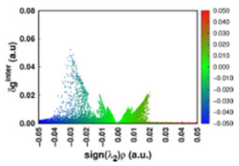	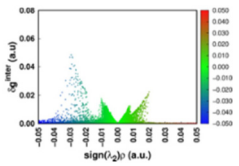	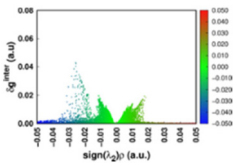	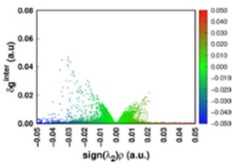
Interaction energy (kcal mol^{-1})	−20.76	−18.08	−21.19	−37.54

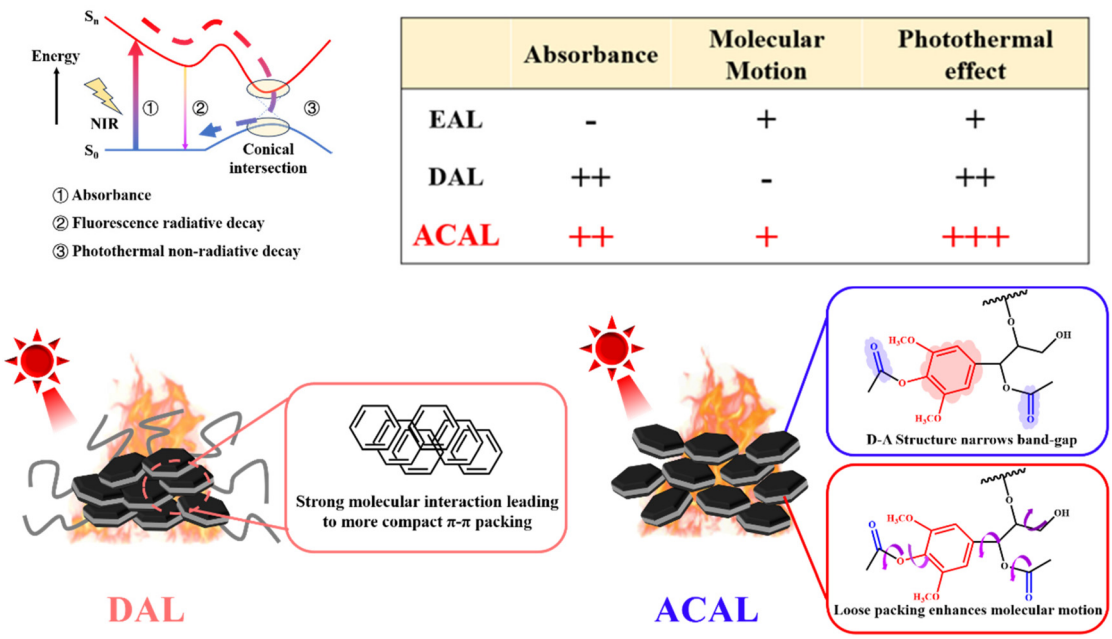

Fig. 9 Mechanism of the enhanced photothermal effect of ACAL.

process and a large quantity of solvent.[27,28,31] In this work, the photothermal effect of lignin was enhanced by simply introducing electron-withdrawing groups and decreasing the intermolecular interaction, rather than enhancing the π–π packing of lignin *via* complex chemical modification and physical assembly processes. The acetylation modification used in this work was a simple reaction and did not involve complex separation and purification processes. The reaction conditions were mild and low-energy consuming. The lignin modification strategies proposed in this paper could enhance the efficient orientation of lignin towards value-added photothermal applications and could help to promote the development of green and environmentally friendly photothermal materials.

4. Conclusion

In this work, the photothermal effect of lignin was significantly enhanced by introducing electron-withdrawing groups. Under the irradiation of an 808 nm laser at 0.81 W cm^{-2}, ACAL exhibited the highest temperature increment of 224 °C. Under 808 nm laser irradiation at 0.51 W cm^{-2}, the photothermal efficiency of ACAL reached as high as 73.2%, which exceeded those of most of the organic photothermal materials. The D–A structure formed by electron acceptor acetyl groups and electron donor aromatic rings narrowed the bandgap and enhanced light absorption of ACAL. The hydroxyl groups of ACAL decreased, leading to the weakened intermolecular inter-

action. Thus, the non-radiative decay of ACAL through molecular motion was enhanced. As both light absorption and non-radiative decay were strengthened, ACAL exhibited the strongest photothermal effect. The strong hydrophobic interaction of dodecyl enhanced the intermolecular interaction in DAL and promoted molecular aggregation, which enhanced light absorption but weakened non-radiative decay through molecular motion. Therefore, the photothermal effect of DAL was weaker than that of ACAL. This work demonstrated an easier regulation strategy to significantly enhance the photothermal effect of lignin *via* simply introducing an electron-withdrawing group (acetyl) and decreasing the intermolecular interaction, rather than enhancing the π–π packing of lignin *via* complex chemical modification and physical assembly processes. The proposed mechanism by which the electron-withdrawing groups enhance the photothermal conversion of lignin indicates that a more elaborate structural design can provide more choices for lignin modifications and broaden the application scenarios of green biomass lignin in the field of value-added photothermal materials.

Conflicts of interest

The authors declare no conflict of interest.

Acknowledgements

This work was supported by the National Natural Science Foundation of China (22078116, 22038004, 22222805, and U23A6005) and the Guangdong Provincial Key Research and Development Program (2020B1111380002).

References

1 Y. Liu, K. Ai, J. Liu, M. Deng, Y. He and L. Lu, *Adv. Mater.*, 2013, **25**, 1353–1359.
2 Y. Liang, X. Zhao, T. Hu, B. Chen, Z. Yin, P. Ma and B. Guo, *Small*, 2019, **15**, 1900046.
3 Z. He, Z. Li, Z. Wang, K. Wang, Y. Sun, S. Wang, W. Wang, Y. Yang and Z. Liu, *Green Chem.*, 2021, **23**, 5775–5785.
4 L. Zhang, H. Du, J. Wang, T. Zhou, J. Guo, X. Li and S. Yu, *Chem. Eng. J.*, 2023, **473**, 145338.
5 S. Gai, G. Yang, P. Yang, F. Hea, J. Lin, D. Jin and B. Xing, *Nano Today*, 2018, **19**, 146–187.
6 S. Xu, X. Bai and L. Wang, *Inorg. Chem. Front.*, 2018, **5**, 751–759.
7 M. Wei, H. Rao, Z. Niu, X. Xue, M. Luo, X. Zhang, H. Huang, Z. Xue and X. Lu, *Coord. Chem. Rev.*, 2021, **447**, 214149.
8 B. Chang, A. Gupta, R. Muthuraj and T. Mekonnen, *Green Chem.*, 2021, **23**, 5337–5378.
9 H. Wang, J. Huang, W. Liu, J. Huang, D. Yang, X. Qiu and J. Zhang, *Macromolecules*, 2022, **55**, 8629–8641.
10 A. Kazzaz, Z. Feizi and P. Fatehi, *Green Chem.*, 2019, **21**, 5714–5752.
11 H. Wang, T. Yuan, G. Song and R. Sun, *Green Chem.*, 2021, **23**, 3790–3817.
12 C. Ma, T. Kim, K. Liu, M. Ma, S. Choi and C. Si, *Front. Bioeng. Biotechnol.*, 2021, **9**, 708976.
13 H. Yang, B. Yu, X. Xu, S. Bourbigot, H. Wang and P. Song, *Green Chem.*, 2020, **22**, 2129–2161.
14 M. Farooq, T. Zou, G. Riviere, M. Sipponen and M. österberg, *Biomacromolecules*, 2019, **20**, 693–704.
15 X. Zhang, W. Liu, D. Yang and X. Qiu, *Adv. Funct. Mater.*, 2018, 1806912.
16 Y. Su, S. Tang, M. Cai, Y. Nie, B. Hu, S. Wu and C. Cheng, *Constr. Build. Mater.*, 2023, **363**, 129863.
17 C. Fang, W. Liu and X. Qiu, *Macromol. Mater. Eng.*, 2019, **304**, 1900257.
18 N. Chen, W. Liu, J. Huang and X. Qiu, *Int. J. Biol. Macromol.*, 2020, **146**, 9–17.
19 T. Zheng, D. Zheng, X. Qiu, D. Yang, L. Fan and J. Zheng, *Cem. Concr. Res.*, 2019, **119**, 89–101.
20 X. Xiao, J. Jiang, Y. Wang, B. Wang, T. Yuan, Q. Shi, X. Liao, B. Shi and R. Sun, *ACS Sustainable Chem. Eng.*, 2021, **9**, 9053–9061.
21 J. Wang, Y. Qian, L. Li and X. Qiu, *ChemSusChem*, 2020, **13**, 4420–4427.
22 X. Lin, P. Wang, R. Hong, X. Zhu, Y. Liu, X. Pan, X. Qiu and Y. Qin, *Adv. Funct. Mater.*, 2022, **32**, 2209262.
23 L. Bai, H. Zhang, R. Lou, J. Li, M. Chi, J. Sha and X. Zhou, *Chem. Eng. J.*, 2023, **455**, 140934.
24 H. Wang, D. Zhu, W. Liu, J. Huang, J. Huang, D. Yang and X. Qiu, *ACS Sustainable Chem. Eng.*, 2023, **11**, 17142–17156.
25 Y. Wang, X. Li, C. Shen, Z. Mao, H. Xu, Y. Zhong, X. Sui, X. Feng and B. Wang, *Int. J. Biol. Macromol.*, 2020, **146**, 1–8.
26 Y. Zhang, D. Yang, X. Qiu and Z. Li, *ACS Appl. Bio Mater.*, 2022, **5**, 5943–5952.
27 Z. Tu, J. Wang, W. Liu, Z. Chen, J. Huang, J. Li, H. Lou and X. Qiu, *Mater. Horiz.*, 2022, **9**, 2613–2625.
28 X. Zhao, C. Huang, D. Xiao, P. Wang, X. Luo, W. Liu, S. Liu, J. Li, S. Li and Z. Chen, *ACS Appl. Mater. Interfaces*, 2021, **13**, 7600–7607.
29 J. Li, W. Liu, X. Qiu, X. Zhao, Z. Chen, M. Yan, Z. Fang, Z. Li, Z. Tu and J. Huang, *Green Chem.*, 2022, **24**, 823–836.
30 Q. Shao, Y. Luo, M. Cao, X. Qiu and D. Zheng, *Chem. Eng. J.*, 2023, **476**, 146678.
31 X. Zhao, L. Shi, B. Tian, S. Li, S. Li, J. Li, S. Li, T. James and Z. Chen, *J. Mater. Chem. A*, 2023, **11**, 12308–12314.
32 Y. He, H. Liao, S. Lyu, X. Xu, Z. Li, I. McCulloch, W. Yue and Y. Wang, *Chem. Sci.*, 2021, **12**, 5177–5184.
33 M. Zha, X. Lin, J. Ni, Y. Li, Y. Zhang, X. Zhang, L. Wang and K. Li, *Angew. Chem., Int. Ed.*, 2020, **59**, 23268–23276.
34 Y. Zou, X. Chen, P. Yang, G. Liang, Y. Yang, Z. Gu and Y. Li, *Sci. Adv.*, 2020, **6**, eabb4696.
35 L. Zhao, Y. Liu, R. Xing and X. Yan, *Angew. Chem., Int. Ed.*, 2020, **59**, 3793–3801.
36 F. Lv, X. Fan, D. Liu and F. Song, *Acta Biomater.*, 2022, **149**, 16–29.

37 C. Xu, R. Ye, H. Shen, J. Lam, Z. Zhao and B. Tang, *Angew. Chem., Int. Ed.*, 2022, **61**, e202204604.
38 Q. Song, Y. Jiao, Z. Wang and X. Zhang, *Small*, 2016, **12**, 24–31.
39 Z. Wang, J. Zhou, Y. Zhang, W. Zhu and Y. Li, *Angew. Chem., Int. Ed.*, 2022, **61**, e202113653.
40 P. Chen, Y. Ma, Z. Zheng, C. Wu, Y. Wang and G. Liang, *Nat. Commun.*, 2019, **10**, 1192.
41 Y. Wang, W. Zhu, W. Du, X. Liu, X. Zhang, H. Dong and W. Hu, *Angew. Chem., Int. Ed.*, 2018, **57**, 3963–3967.
42 W. Hu, X. Miao, H. Tao, A. Baev, C. Ren, Q. Fan, T. He, W. Huang and P. Prasad, *ACS Nano*, 2019, **13**, 12006–12014.
43 Y. Wang, G. Xia, M. Tan, M. Wang, Y. Li and H. Wang, *Adv. Funct. Mater.*, 2022, **32**, 2113098.
44 T. Dong, K. Wen, J. Chen, J. Xie, W. Fan, H. Ma, L. Yang, X. Wu, F. Xu, A. Peng and H. Huang, *Adv. Funct. Mater.*, 2018, **28**, 1800135.
45 M. Su, Q. Han, X. Yan, Y. Liu, P. Luo, W. Zhai, Q. Zhang, L. Li and C. Li, *ACS Nano*, 2021, **15**, 5032–5042.
46 D. Xi, M. Xiao, J. Cao, L. Zhao, N. Xu, S. Long, J. Fan, K. Shao, W. Sun, X. Yan and X. Peng, *Adv. Mater.*, 2020, **32**, 1907855.
47 Z. Zhao, C. Chen, W. Wu, F. Wang, L. Du, X. Zhang, Y. Xiong, X. He, Y. Cai, R. Kwok, J. Lam, X. Gao, P. Sun, D. Phillips, D. Ding and B. Tang, *Nat. Commun.*, 2019, **10**, 768.
48 Z. Jiang, C. Zhang, X. Wang, M. Yan, Z. Ling, Y. Chen and Z. Liu, *Angew. Chem., Int. Ed.*, 2021, **60**, 22376–22384.
49 S. Liu, X. Zhou, H. Zhang, H. Ou, J. Lam, Y. Liu, L. Shi, D. Ding and B. Tang, *J. Am. Chem. Soc.*, 2019, **141**, 5359–5368.
50 V. Passoni, C. Scarica, M. Levi, S. Turri and G. Griffini, *ACS Sustainable Chem. Eng.*, 2016, **4**, 2232–2242.
51 M. Johansson, M. Skrifvars, N. Kadi and H. Dhakal, *Ind. Crops Prod.*, 2023, **202**, 117049.
52 L. Szabó, R. Milotskyi, H. Ueda, T. Tsukegi, N. Wada and K. Takahashi, *Chem. Eng. J.*, 2021, **405**, 126640.
53 F. Chen, H. Dai, X. Dong, J. Yang and M. Zhong, *Polym. Compos.*, 2011, **32**, 1019–1025.
54 B. Li, S. You, W. Qia, Y. Wang, R. Su and Z. He, *Eur. Polym. J.*, 2020, **126**, 109539.
55 J. Wen, S. Sun, B. Xue and R. Sun, *Materials*, 2013, **6**, 359–391.
56 K. Cheng, H. Sorek, H. Zimmermann, D. Wemmer and M. Pauly, *Anal. Chem.*, 2013, **85**, 3213–3221.
57 L. Chen, Y. Shi, B. Gao, Y. Zhao, Y. Jiang, Z. Zha, W. Xue and L. Gong, *ACS Sustainable Chem. Eng.*, 2020, **8**, 714–722.

